Medical Implants and Devices: Numerical modeling of galvanic corrosion problems of dental implants screws and nuts via BEM

Dimitrios T. Kalovelonis, Department of Mechanical Engineering and Aeronautics, University of Patras, GR-26500, Patras, Greece. d.kalovelonis@upnet.gr

Abstract

Corrosion is of great concern particularly when a metallic implant is placed in the hostile electrolytic environment of the human body. The implants face severe corrosion environment which includes blood and other constituents of the body fluids. The aqueous medium in the human body consists of various anions such as chloride, and dissolved oxygen. Changes in the pH values also influence corrosion. Though, the pH value of the human body is normally maintained at 7, this value changes from 3 to 9 due to several causes such as accidents, diseases, infections, and other factors. Oral implants, screws and nuts are either different grades of stainless steels alloys, either stainless steel and titanium alloys, or stainless steel and cobalt–chromium–molybdenum alloys galvanic couples. The boundary element method (BEM) is ideal for solving galvanic corrosion problems. In the present work the effect of pH, temperature, and electrical conductivity on the galvanic corrosion of oral implants screws and nuts is studied, using BEM.

1. Introduction

Metallic implants corrode when are placed in the human body, due to the presence of blood and other constituents of the body fluids like water, sodium, chlorine, proteins, plasma, amino acids along with mucin in the case of saliva (Kubie& Shults, 1925). The aqueous medium in the human body consists of various anions such as chloride, phosphate, and bicarbonate ions, cations, organic substances of low-molecular-weight species as well as relatively high molecular-weight polymeric components, and dissolved oxygen (Scales et. al., 1959; Williams, 1978). Changes in the pH values also influence corrosion. Though, the pH value of the human body is normally maintained at 7, this value changes from 3 to 9 due to several causes such as accidents, imbalance in the biological system due to diseases, infections, and other factors. After surgery the pH value near the implant varies typically from 5.3 to 5.6 (Manivasagam et. al., 2010).

Dental implant fixtures have become an integral part of treatment for partially or fully edentulous patients since Branemark introduced the two-stage treatment protocol (Brånemark et. al., 1969). Commercially pure titanium and its alloys have been widely used for dental implants due to their mechanical properties, good corrosion resistance in biological fluids and biocompatibility (Balkin, 1988). Although is widely accepted that titanium alloys are good materials for endoosseous implantation, the choice of a suitable alloy for the suprastructure still remains an open question (Al-Mayouf et. al.,2004). Oral implants corrode due their contact with saliva that disrupts the passive film, creating galvanic cells (Mellado-Valero et.al., 2018). Dental implants, screws and nuts are either different grade of stainless steel, titanium, cobalt-chromium, and cobalt–chromium–molybdenum alloys (Manivasagam et. al., 2010). Those alloys form galvanic couples.

Galvanic corrosion is caused due to the potential difference established when two metals (alloys) are electrically connected in a conducting medium, and produces electron flow causing the metal (alloy) with more negative potential to preferentially corrode (anode) and the more positive metal (alloy) to become a cathode and to be protected by the negative metal (alloy). Galvanic corrosion also occurs when the same metal is in contact with an electrolyte at two different concentrations or with different aeration levels (differential aeration cell). For example, electrolyte with varying pH, temperature etc. in contact with a structure, creates galvanic cells (Popov, 2015).

Complicated electrochemical processes related to implant and suprastructure are linked to galvanic corrosion (Venugopalan & Lucas, 2018; Geis-Gerstorfer et.al., 1989) which leads to clinically relevant situations, due to the biological effects, that may result from the dissolution of alloy components, or caused by the current flow from galvanic coupling, resulting in bone destruction. For example, galvanic coupling could result in an electropositive local environment along the implant interface, which could directly influence bone resorption (Lucas & Lemons, 1992). Furthermore, the ionic release induced by corrosion could be responsible for peri-implantitis and treatment failure (Olmedo et. al., 2003). In addition, the corrosion products can be distributed throughout the entire body and cause allergic reactions or a hypersensitivity reaction (Geis-Gerstorfer et.al., 1989). Also, the corrosion process may limit the metals resistance to fatigue resulting in the fracture of the implant (Guglielmotti & Cabrini, 1997).

The boundary element method (BEM) has been used extensively in galvanic corrosion problems (Danson & Warne, 1983; Deconinck et. al. 1985; Aoki & Kishimoto, 1990; Gulikers & Raupach, 2006; Warkus & Raupach 2006,2010). BEM is ideal for solving galvanic corrosion problems, since it offers the advantages of dimensionality reduction of the problem by one, and the high accuracy of the solution of the electric potential gradients. In the last decades, the BEM has become much more attractive to use by overcoming the disadvantages of time-consuming computations and the high demand for computer memory, utilizing acceleration techniques such as fast multipole (Keddie et.al., 2007; Liu, 2009) and adaptive cross approximation (Rodopoulos et. al., 2019; Gortsas et. al., 2021; Kalovelonis et. al.,2020, 2022, 2023). With these techniques, it is possible to efficiently solve large-scale CP engineering problems with million degrees of freedom in a standard workstation (Rodopoulos et. al., 2019; Gortsas et. al., 2021; Kalovelonis et. al.,2020, 2022, 2023).

In the present work the application of BEM to galvanic corrosion problems of dental implants screws and nuts is presented. The present work is organized as follows. Section 2 briefly describes the galvanic corrosion of dental implants screws and nuts. Section 3 describes the mathematical modelling of corrosion problems. Section 4 concerns the modeling of the boundary conditions. Section 5 presents BEM formulations. Finally, the main conclusions are provided in Section 6.

2. Galvanic corrosion of dental implants screws and nuts

Dental implant screws and nuts consist of the dental implant body, i.e., the screw, the dental implant suprastructure or abutment, and the crown or artificial tooth (Kandavalli et. al., 2021) as depicted in fig. (1).

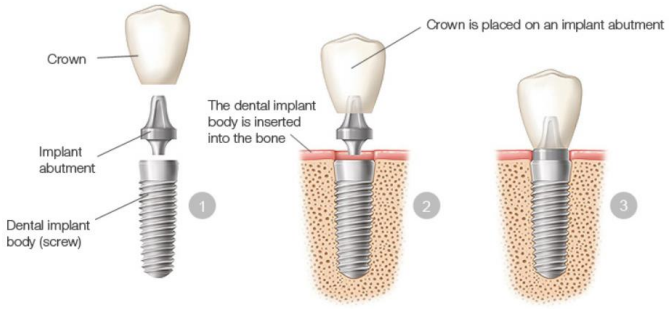

***Figure 1**. Description of dental implants*

It is widely accepted that titanium alloys, such as Ti6Al4V, are good materials for endoosseous implantation, due to their mechanical properties, good corrosion resistance in biological fluids and biocompatibility (Balkin, 1988), although the choice of a suitable alloy for the suprastructure still remains an open question (Al-Mayouf et. al.,2004). Typical materials used for the suprastructure amongs others are CoCr, CoCrMo, SS304 and SS316 (Manivasagam et. al., 2010). Implants corrode due their contact with saliva that disrupts the passive film (Nagay et. al., 2022), as shown in fig. (2), creating galvanic cells.

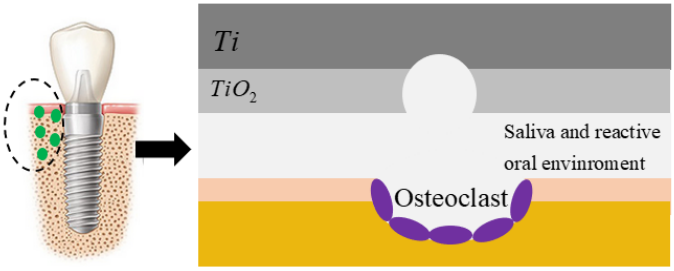

***Figure 2**. Corrosion of dental implants*

Galvanic corrosion occurs due to the potential difference established when two metals (alloys) are electrically connected in a conducting medium, producing electron flow and causes the metal (alloy) with more negative potential to preferentially corrode (anode), and the more positive metal (alloy) to become a cathode and to be protected by the negative metal (alloy). Galvanic corrosion also occurs when the same metal is in contact with an electrolyte at two different concentrations or with different aeration levels (differential aeration cell). For example, electrolyte with varying pH, in contact with a structure, creates galvanic cells. In figs (3a) and (3b) a schematic description of the galvanic corrosion principles is shown.

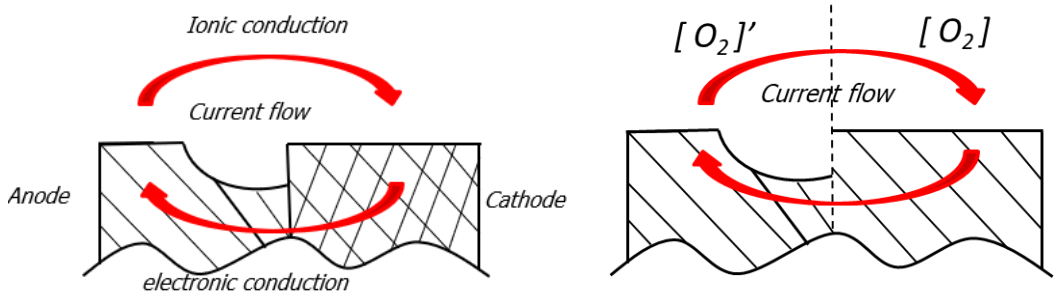

(a) (b)

***Figure 3**. Galvanic corrosion due to a) potential difference and b) difference in oxygen concentration*

3. Mathematical modeling of corrosion problems

In dilute solutions, the transport of species, is due to migration (fig. (4a)), diffusion (fig. (4b)), and fluid flow, and governed by the Nernst-Planck (N-P) equations (Newman & Thomas-Alyea, 2004):

$$\frac{\partial c_i}{\partial t} + \mathbf{v}\cdot\nabla c_i = z_i F \nabla\cdot\left(u_i c_i \nabla\varphi\right) + \nabla\cdot\left(D_i \nabla c_i\right) + A_i \tag{1a}$$

$$\mathbf{J} = F\sum z_i \mathbf{N}_i \tag{1b}$$

$$\mathbf{N}_i = -D_i\nabla c_i - z_i F u_i c_i \nabla\varphi$$

where c_i is the concentration of i^{eth} species, **v** is the electrolyte velocity., z_i is the number of electrons taking part in an electrochemical reaction, u_i is the mobility, φ is the electric potential, D_i is the diffusivity, *Ai* the production term, **J** is the current density vector and **N** is the flux vector.

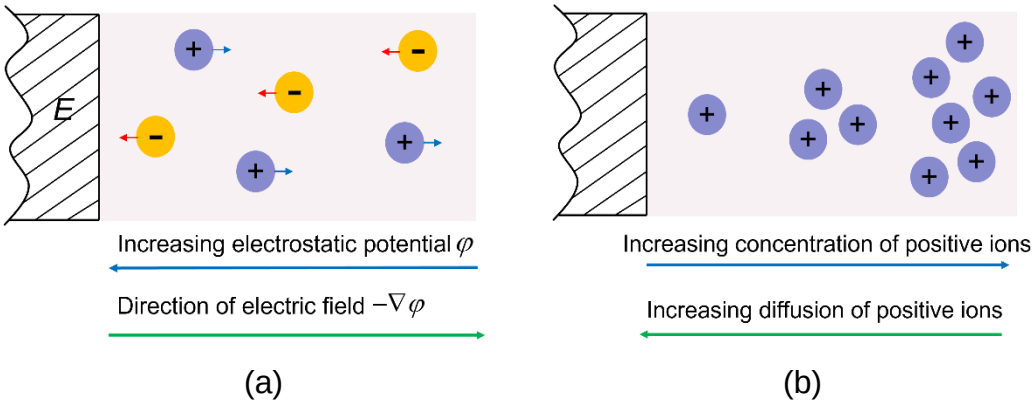

Figure 4*. transport of species in dilute electrolyte due to a) migration and b) diffusion*

Furthermore, the electric potential is governed by the electrostatic equation:

$$\nabla^2\varphi = -\frac{1}{\varepsilon}F\sum z_i c_i \tag{2}$$

where *F* is the Faraday constant.

Due to the migration, diffusion and electrolyte flow, it is formed an interphase, called the electric double layer (EDL), where chemical reactions such as metal dissolution and oxygen reduction occur (Bockris et.al., 2000). The EDL structure of a metal in water is depicted in figs.(5a) and (5b). The metallic surface has a current q

and is occupied by unsolvated negative ions and water molecules. In the inner Helmholtz plane (IHP) a net current q_1 exists and is occupied by solvated positive ions. The outer Helmholtz plane (OHP) and the diffuse layer are occupied by negative ions and water molecules. In comparison with the OHP the diffuse layer is a dilute solution with net current q_2 (Bockris et.al., 2000; Newman & Thomas-Alyea, 2004).

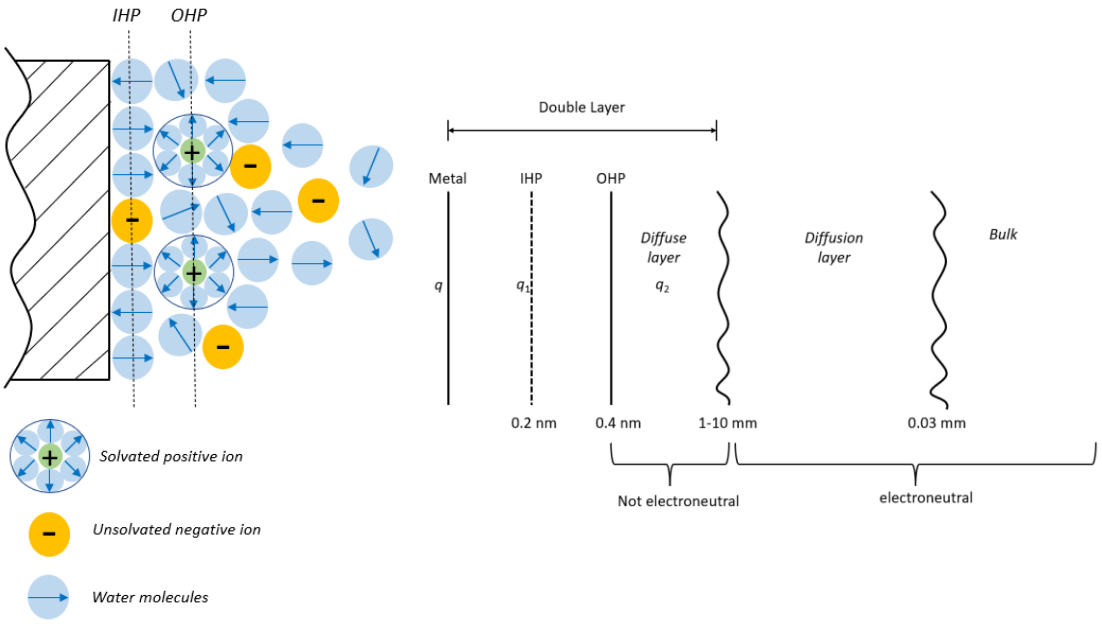

(a) (b)

***Figure 5**. The EDL structure (a) of metal in water, and (b) its description*

In the region between the metallic surface and the OHP the movement of species is due to forces from ion-ion interaction (Bockris et.al., 2000), and the N-P equations does not hold. Molecular dynamics simulations are applied in the above-described region (Bockris et.al., 2000). Moving away from the EDL, a region called the diffusion layer exists, where it has zero net current (Bockris et.al., 2000). Electrolytes with zero net current are called electroneutral and the electroneutrality condition holds:

$$\sum z_i c_i = 0 \qquad (3)$$

In the case of electrically balanced reactions, the sum of the production rates becomes zero, i.e.:

$$\sum z_i A_i = 0 \tag{4}$$

Multiplying Eq (1a) with Fz_i and taking the sum of Eq. (1a) for all species, the following equation is derived:

$$\frac{\partial}{\partial t}\left(F\sum z_i c_i \right) = -\nabla \cdot \left(F\sum z_i \mathbf{N}_i \right) + F\sum z_i A_i \tag{5}$$

Combining eqs. (3)-(5), the charge conservation equation is produced:

$$\nabla \cdot \mathbf{J} = 0 \tag{6}$$

Eq. (6) states that in electroneutral solutions charge conservation holds. Typically, the concentration variation in a solution is as depicted in figure (6).

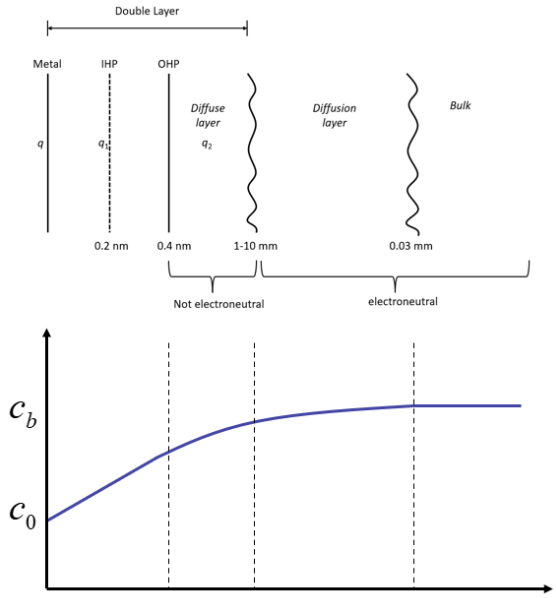

***Figure 6**. Typical concentration distribution*

Moving away from the diffusion layer, the bulk of the solution exists (Newman & Thomas-Alyea, 2004), where the electrolyte is neutral, and concentration of the species is uniform. From eq. (6) the following equation can be derived:

$$\nabla \cdot \left(F^2 \sum z_i^2 u_i c_i \nabla \varphi \right) - F \sum z_i \nabla \cdot \left(D_i \nabla c_i \right) = 0 \qquad (7)$$

If the electrical conductivity σ is constant, then eq. (7) is reduced to the Laplace equation:

$$\nabla^2 \varphi = 0 \qquad (7)$$

Consider an electrolyte, where two metals exist, one that plays the role of the anode with surface S_a (green line), and another that plays the role of the cathode with surface S_c (red line), the electrolyte can be enclosed either by physical or fictitious boundaries with surface S_b (black line) as depicted in fig. (7).

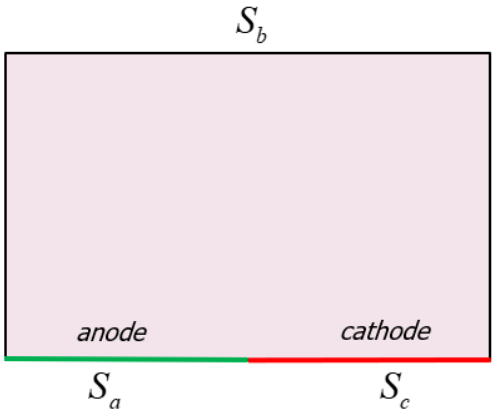

***Figure 7**. Description of a corrosion problem*

In the anodic and cathodic boundaries, non-linear expressions between the normal current density on the surface and the concentration and potential values on the surface, called polarization curves are applied. On the physical or fictitious boundaries, for the N-P equations insultation boundary conditions, Newmann or Dirichlet conditions are applied for each species concentration field. The above-described boundary conditions for the N-P equations are summarized as follows (Newman & Thomas-Alyea, 2004):

$$-Fz_k D_k \mathbf{n} \cdot \nabla c_k(\mathbf{x}) - F^2 z_k^2 u_k c_k(\mathbf{x}) \mathbf{n} \cdot \nabla \varphi(\mathbf{x}) = f_k(c_k(\mathbf{x}), \varphi(\mathbf{x})) \ , \ \mathbf{x} \in S_c \qquad (8)$$

$$-Fz_k D_k \mathbf{n} \cdot \nabla c_k(\mathbf{x}) - F^2 z_k^2 u_k c_k(\mathbf{x}) \mathbf{n} \cdot \nabla \varphi(\mathbf{x}) = g_k(c_k(\mathbf{x}), \varphi(\mathbf{x})) \ , \ \mathbf{x} \in S_a \qquad (9)$$

$$c_k(\mathbf{x}) = c_k^b \ , \mathbf{x} \in S_b \tag{10}$$

$$\mathbf{n} \cdot \nabla c_k(\mathbf{x}) = p_k \ , \mathbf{x} \in S_b \tag{11}$$

$$c_k(\mathbf{x},t) = c_k^b(t) \ , \mathbf{x} \in S_b \tag{12}$$

$$\mathbf{n} \cdot \nabla c_k(\mathbf{x},t) = p_k(t) \ , \mathbf{x} \in S_b \tag{13}$$

One or some of eqs. (10) – (12) could be applied on the physical or fictitious boundaries, on several subsets of those boundaries, regarding to each specific problem. For the Laplace equation the following boundary conditions can be applied (Rodopoulos et. al., 2019; Gortsas et. al., 2021; Kalovelonis et. al.,2020, 2022, 2023):

$$-\sigma \mathbf{n} \cdot \nabla \varphi(\mathbf{x}) = h_k(\varphi(\mathbf{x})) \ , \mathbf{x} \in S_c \tag{14}$$

$$-\sigma \mathbf{n} \cdot \nabla \varphi(\mathbf{x}) = t_k(\varphi(\mathbf{x})) \ , \mathbf{x} \in S_a \tag{15}$$

$$\mathbf{n} \cdot \nabla \varphi(\mathbf{x}) = 0 \ , \mathbf{x} \in S_b \tag{16}$$

4. Polarization curves

The corrosion rate of metallic and alloys oral implants in an electrolyte, in the human body is influenced by various parameters. Amongst other these are the temperature, pH, oxygen and chlorides concentration of the solution, the presence of fluorides and microorganisms, the dental plaque, mechanical stresses, the alloy composition etc (Nagay et. al., 2022). To model efficiently corrosion models, the above-described parameters should be incorporated into the boundary conditions. For the N-P equations the boundary condition on the metallic surface, for each species, is equal to the rate of the partial reaction that the species participate. For the Laplace and Poisson equations the boundary condition on the metallic surface is the sum of the anodic and cathodic partial reactions rates that occur in the electrode surface, i.e., the polarization curve. A typical polarization curve is depicted in fig. (8).

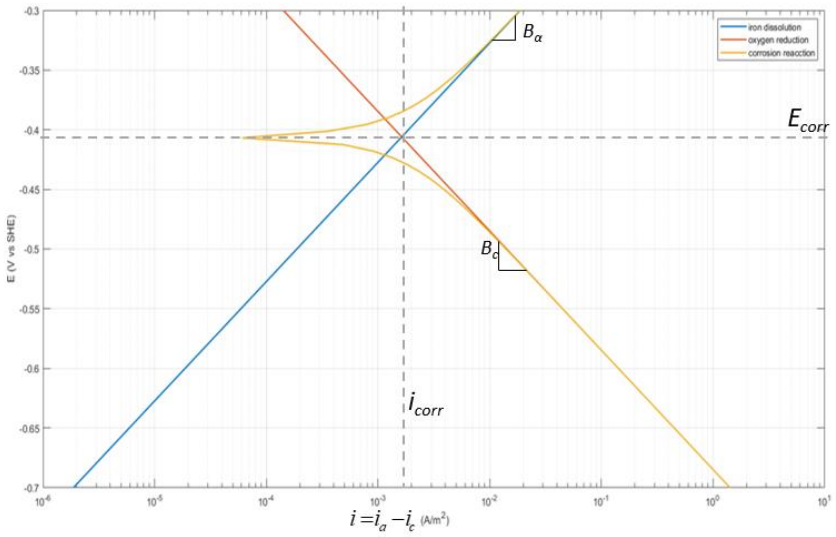

***Figure 8**. Typical polarization curve*

In general metals and alloys immersed in an electrolyte exhibit active-passive behavior (Popov, 2015). Their polarization is divided in four regions, the transpassive, passive, transition and active regions. A typical active-passive anodic partial reaction curve is depicted in fig. (9).

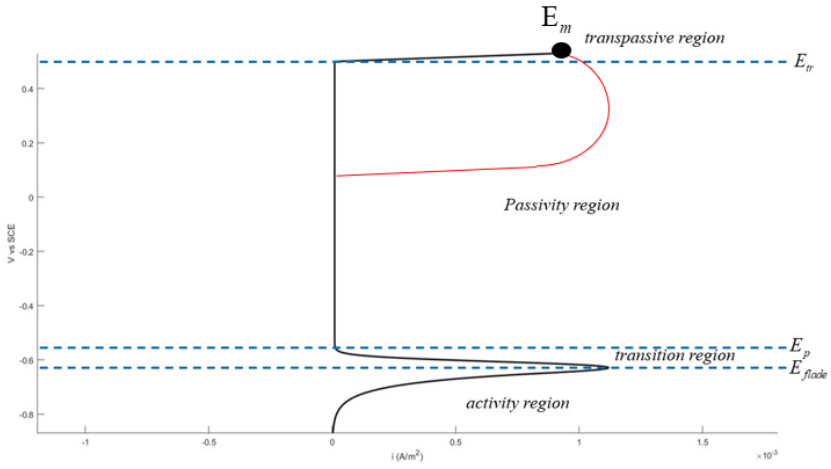

***Figure 9**. Typical active-passive anodic partial reaction curve*

In the transpassive region, for potentials larger than the transpassivation or pitting potential E_{tr} pitting corrosion occurs. The anodic partial reaction rate is given by the following expression (Flitt & Schweinsberg, 2005):

$$i_{Fe,trp}(\varphi) = i_p \frac{1+e^{\frac{E_m - E_{br} - \varphi}{b_{tr}}}}{e^{\frac{E_m - E_{br} - \varphi}{b_{tr}}}} \quad (17)$$

where E_m is the maximum potential found and b_{tr} is the transpassive region slope. The transpassivation potential is the potential which pitting corrosion starts to occur and is affected by the chloride and hydroxyls concentration on the alloy surface (Macdonald et. al., 2021):

$$\mathrm{E}_{tr} = a - b\log(c_{Cl^-} / c_{OH^-}) \quad (18)$$

where a and b are constants, i.e., the transpassivation potential decreases with the increase of chloride content, in the metallic surface. In the passive region, the passive film on the surface of the alloy, is sustained, and the metal does not corrode. The passive region ranges for potential between the passivation potential E_p and the transpassivation potential E_{tr}. The passivation potential is influenced by the composition of the metal, temperature and pH of the solution on the surface of the alloy. The passive current density increases with the increase of temperature, pH and chlorides on the surface of the alloy, and is given by the following expression (Macdonald et. al., 2020):

$$i(\varphi) = i_p(T, pH, [Cl^-]) = a_0\ i_p(298.15, 13.5, 0)\ e^{-a_1\left(\frac{1}{T} - \frac{1}{298.15}\right)}\ e^{a_2(pH-13.5)}\ e^{a_3[Cl^-]} \quad (19)$$

where a_i are constants, and T is the temperature. The transition region is an unstable region, and eventually steel will become either active or passive. In the transition region, Hines (Hines, 1983) assumed that two rates exist, one where metal dissolution occurs, and another where film deposits. The transition region is defined within the potential limits of the Flade potential E_{pp}, which is the upper limit of the activity region, and the passivation potential Ep. The corrosion rate then is:

$$i_{a,up}(\varphi) = S i_{a,act}(\varphi, c) + (1-S) i_{ss}(\varphi) \quad (20)$$

Where S is the metal fraction that steel dissolution occurs. Initially Hines (Hines, 1983) proposed two expressions for the metal fraction, later Flitt and Schweinsberg (Flitt & Schweinsberg, 2005) proposed a more accurate one:

$$S = 2\frac{e^{-A\left(E_{flade}-E_p\right)^p}}{1+e^{-A\left(E_{flade}-E_p\right)^p}} \tag{21}$$

The values of the parameters p and A are given in the literature (Flitt & Schweinsberg, 2005). For the stainless-steel alloys, the Flade potential is a function of pH and chromium concentration (Revie & Uhlig, 2008):

$$E_{flade} = E^0_{flade}([Cr]) - 0.059\,pH \tag{22}$$

The dependency of chromium composition can be found in the literature (Frank, 1949; King & Uhlig, 1959; Rocha & Lennartz, 1955). The increase of chromium content causes a decrease on the Flade potential of stainless steel. In the activity region, active dissolution of steel occurs with rate (Popov, 2015):

$$i_{Fe,act}\left(\varphi\right) = i^0_{Fe} e^{\frac{\varphi - E_{eq,Fe}}{b_{Fe}}} \tag{23}$$

Where b_{Fe} is the iron dissolution Tafel slope, $E_{eq,Fe}$ is the iron equilibrium potential, and i^o_{Fe} is the iron dissolution exchange current density. Iron equilibrium potential variation with pH can be found using iron's Pourbaix diagram (Pourbaix, 1974).

$$E_{eq,Fe} = -0.441 - \frac{RT}{2F}\log\left(Fe^{++}\right) \tag{24}$$

Where F is the Faraday constant. The rate of the cathodic partial reaction is given by the Eq (25) activation and concentration polarization (Popov, 2015)::

$$i_{O_2}\left(\varphi\right) = \frac{i^0_{O_2} e^{\frac{\varphi - E_{eq,O_2}}{b_{O_2}}}}{1+\left(\frac{i^0_{O_2}}{i_{\lim,O_2}}\right)e^{\frac{\varphi - E_{eq,O_2}}{b_{O_2}}}} \tag{25}$$

Where b_{O2} is the oxygen reduction Tafel slope, $E_{eq,O2}$ is the oxygen equilibrium potential, i^o_{O2} is the oxygen reduction exchange current density, and $i_{lim,O2}$ is the oxygen limiting current density, which corresponds to the complete oxygen depletion in the solution layer adjacent to the metallic surface. Various models for the limiting

current density calculation can be found in the literature, such as Peers (Peers ,1956), Leveque (Newman & Thomas-Alyea, 2004) and Nakayama (Nakayama et.al., 2017) amongst others. The equilibrium potential of oxygen reduction is a function of pH and temperature (Popov, 2015):

$$E_{eq,O_2} = E_{0,O_2}(T) + \frac{RT}{zF}(14 - pH) \tag{26}$$

The Tafel slope is calculated as follows (Popov, 2015):

$$b_i = \frac{RT}{a_i zF} \tag{27}$$

where α_i is the is the fraction of the total free energy that decreases the energy barrier for the partial reaction. The exchange current density is given by the following expression (Popov, 2015)::

$$i_i^0 = FAk_0 C_i^b e^{\frac{E_{eq,i} - E_{0,i}}{b_i}} \tag{28}$$

Where k_0 is standard reaction rate constants, E_0 is the standard electromotive force, c^b is the bulk concentration, and A is the electrode surface. Finally, the pH can be calculated by Eqs. (29) or (30) (Popov, 2015):

$$pH = -\log\left([H^+]\right) \tag{29}$$

$$pH = pK_w + \log\left([OH^-]\right) \tag{30}$$

Where pK_w is the autoionization process rate constant. The influence of chloride content, chromium concentration and pH in anodic and cathodic partial reaction rates is depicted in Figs. 10(a) and 10(b).

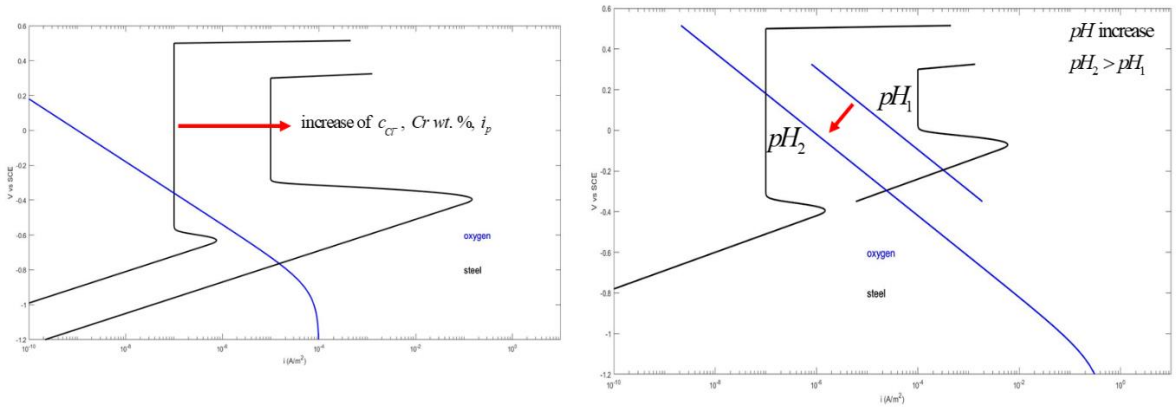

(a) (b)

***Figure 10**. Effect of a) chloride content and chromium concentration and b) pH on partial anodic and cathodic reactions rates*

The influence of the Tafel slope, equilibrium potential, exchange current density and limiting current density, on the reaction rates is depicted in figs. (11(a)) and (11(b)).

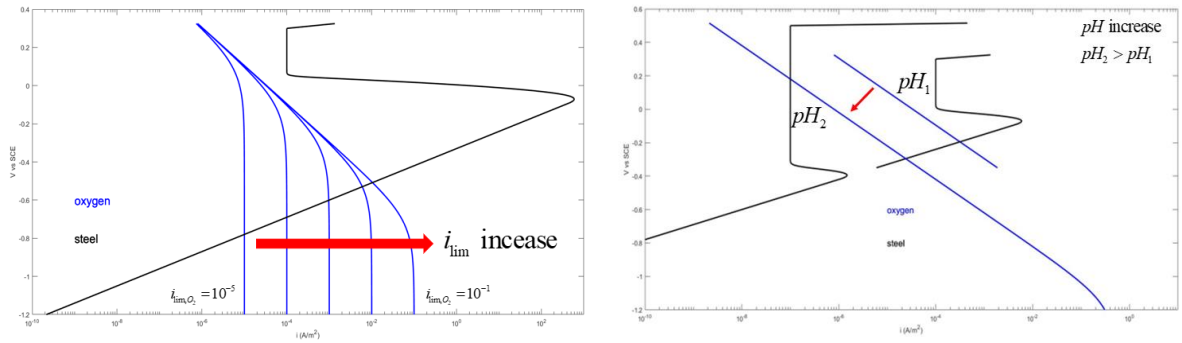

(a) (b)

***Figure 11**. Effect of a) limiting current density and b) Tafel slope, equilibrium potential and exchange current density on the reaction rates*

5. BEM for corrosion problems

In this section an accelerated BEM formulation for the Laplace and Poisson equations, and a Local Domain BEM (LD-BEM) formulation for the N-P equations are presented.

5.1 Accelerated BEM for the Laplace and Poisson equations

Consider an electrolyte, where two metals exist, one that plays the role of the anode with surface S_a (red line), and another that plays the role of the cathode with surface S_c (green line), the electrolyte can be enclosed either by physical or fictitious boundaries with surface S_b (black line) as depicted in fig. (7). The integral form of Eq. (7) reads (Telles et.al., 1984):

$$a(\mathbf{x})\varphi(\mathbf{x}) + \int_S \partial_n G(\mathbf{x},\mathbf{y})\varphi(\mathbf{y})\,dS_y = \int_S G(\mathbf{x},\mathbf{y})\partial_n\varphi(\mathbf{y})\,dS_y \tag{31}$$

where $S = S_p \cup S_{f_1} \cup S_{f_2}$, $\alpha(\mathbf{x})$ is a coefficient that depends on the local smoothness of the surface, **x** and **y** are points that lie on the surface S, $G(\mathbf{x},\mathbf{y})$ is the full space fundamental solution of the Laplace equation, and $\partial_n G(\mathbf{x},\mathbf{y})$ is its normal derivative given in three dimensions by the following expressions (Telles et.al., 1984):

$$\begin{aligned} G(\mathbf{x},\mathbf{y}) &= \frac{1}{4\pi|\mathbf{r}|} \\ \partial_n G(\mathbf{x},\mathbf{y}) &= -\frac{1}{4\pi|\mathbf{r}|^3}\mathbf{r}\cdot\hat{\mathbf{n}} \\ \mathbf{r} &= \mathbf{y} - \mathbf{x} \end{aligned} \tag{32}$$

The boundaries S are discretized into quadrilateral or/and triangular surface elements. In each element, the fields $\varphi(\mathbf{x})$ and $\partial_n\varphi(\mathbf{x})$ are assumed to be constant. Then, the boundary integral equation (31), written for the collocation point located at the center of the element i, obtains the following discrete form:

$$\frac{1}{2}\varphi^i + \sum_{e=1}^{E} H_{ie}\varphi^e = \sum_{e=1}^{E} G_{ie} q^e \tag{33}$$

where E denote the total number of elements, the symbol q indicates potential flux ($q = \partial_n\varphi$), while the integrals H and G have the form:

$$H_{ie} = \int_{-1}^{1}\int_{-1}^{1} \partial_n G\left(\mathbf{x}^i, \mathbf{y}^e(\xi_1,\xi_2)\right)\left|\mathbf{J}^e\right| d\xi_1 d\xi_2 \tag{34}$$

$$G_{ie} = \int_{-1}^{1}\int_{-1}^{1} G\left(\mathbf{x}^i, \mathbf{y}^e(\xi_1,\xi_2)\right)\left|\mathbf{J}^e\right| d\xi_1 d\xi_2 \tag{35}$$

where $\mathbf{J}^e$ stands for the Jacobian matrix of the transformation from the global Cartesian to the local coordinate system. The integrals of Eqs. (34) and (35) are evaluated numerically via highly accurate, direct integration techniques illustrated in (Polyzos et. al., 1998). Boundary conditions (14) and (15) (polarization curves) correlate the potential with the current density in a non-linear way. For the solution of the system of algebraic equations (33), an iterative Newton-Raphson procedure is applied. According to the Newton-Raphson scheme, Eq. (14) becomes:

$$\partial_n \varphi^k(\mathbf{x}) = -\frac{1}{\sigma} f\left(\varphi^{k-1}(\mathbf{x})\right) - \frac{1}{\sigma} \frac{\partial f\left(\varphi^{k-1}(\mathbf{x})\right)}{\partial \varphi} \Delta\varphi^k(\mathbf{x}) \tag{36}$$

$$\varphi^k(\mathbf{x}) = \varphi^{k-1}(\mathbf{x}) + \Delta\varphi^k(\mathbf{x}) \tag{37}$$

where the index k represents the Newton-Raphson iteration step. Similar equations are obtained for the polarization curve of Eq. (15). Rearranging Eq. (33) with the aid of Eqs. (36) – (37), the linear boundary condition of Eqs. (16) the following linear algebraic system of equations, is produced, for each iteration k:

$$\left[\mathbf{A}^{k-1}\right] \cdot \left\{\mathbf{X}^k\right\} = \left\{\mathbf{B}^{k-1}\right\} \tag{38}$$

Finally, the linear algebraic system of Eq. (38) is solved, for each iteration k, by means of the iterative GMRES solver with a chosen accuracy $\varepsilon_{\text{GMRS}}$. The iterative solution is accelerated by a hierarchical LU preconditioner with a chosen accuracy ε_{LU} (Rodopoulos et.al., 2019; Gortsas et.al., 2021)

Using the above-described BEM formulation, the galvanic corrosion problem of fig. (7) is solved, with anode and cathode length 0.5 and 1 respectively (1.5 total length), using as boundary conditions the polarization curves shown in fig. (12).

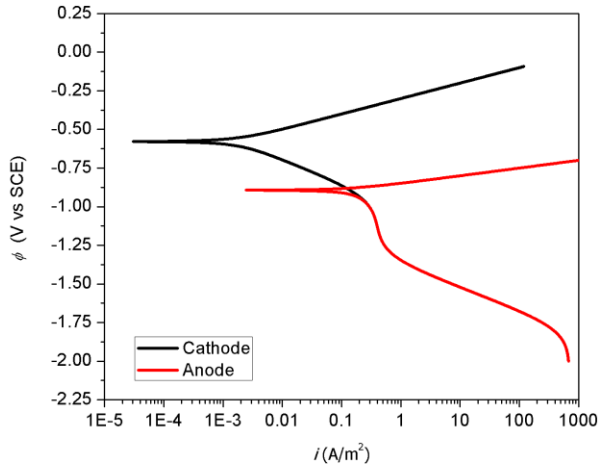

***Figure 12**. Polarization curves of the above-described galvanic corrosion problem*

In figs. (13(a)) and (13(b)) the potential and current density distributions are depicted. In the cathodic surface a potential drop is observed, while a potential increase from the equilibrium state, at the anodic surface is observed. Furthermore, as expected the current density values in the cathodic surface are negative (cathodic), while at the anodic surface are positive (anodic).

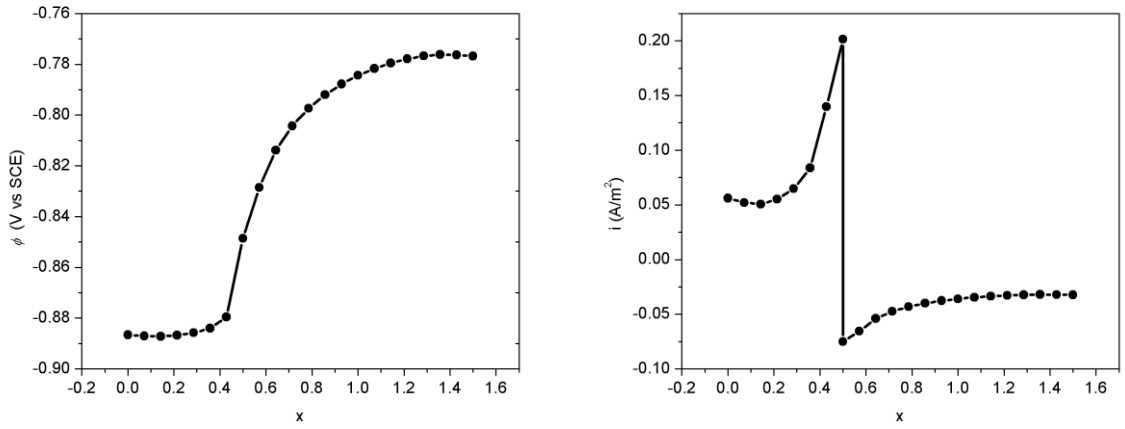

(a) (b)

***Figure 13**. a) Potential and b) current density distribution at the anodic and cathodic surfaces*

5.2 LD-BEM for the N-P equations

Recently Gortsas et. al. proposed the local domain boundary element method (LD-BEM), for fisher diffusion(Gortsas et. al., 2022) and convection-diffusion problems with constant velocity (Gortsas & Tsinopoulos, 2022), which exhibits computational complexity of the same order with the finite element method. LD-BEM has the advantages of high accuracy of the solution of the concentration gradients and the efficient treatment of the non-linear boundary conditions. In electroneutral electrolytes the N-P equations, can be written as convection-diffusion equations, since eq. (1a) can be written:

$$\frac{\partial c_1}{\partial t} + \mathbf{v} \cdot \nabla c_1 + (-Fz_1u_1\nabla\varphi) \cdot \nabla c_1 - (Fz_1u_1\nabla^2\varphi)c_1 - D_1\nabla^2 c_1 + A_1 = 0 \tag{39}$$

Assuming first order reaction rates, and due to electroneutrality then:

$$\frac{\partial c_1}{\partial t} + \mathbf{v}_t \cdot \nabla c_1 - D_1\nabla^2 c_1 - kc_1 = 0 \tag{40}$$

with $\mathbf{v}_t = \mathbf{v} + \mathbf{v}_e$, where $\mathbf{v}_e$ is defined as follows:

$$\mathbf{v}_e = -Fz_1u_1\nabla\varphi \tag{41}$$

In the absence of fluid flow or in the present of a uniform velocity field, in order the convection-diffusion LD-BEM formulation of Gortsas & Tsinopoulos (Gortsas & Tsinopoulos, 2022). to be valid for corrosion problems, the potential gradient values should also be constant. To examine the potential gradient field behavior in galvanic corrosion problems, the potential gradient values are calculated for the galvanic corrosion problem of the previous section, using the following expression (Wrobel, 2002):

$$\nabla\varphi = \int_{S_a \cup S_c \cup S_b} \nabla_{\mathbf{x}} Q(\mathbf{x},\mathbf{y})\varphi(\mathbf{y})\, dS_{\mathbf{y}} + \int_{S_a \cup S_c \cup S_b} \nabla_{\mathbf{x}} G(\mathbf{x},\mathbf{y})\partial_n\varphi(\mathbf{y})\, dS_{\mathbf{y}} \tag{42}$$

where

$$\nabla_{\mathbf{x}} G(\mathbf{x},\mathbf{y}) = \frac{\mathbf{r}}{4\pi|\mathbf{r}|^3}$$

$$\nabla_{\mathbf{x}} Q(\mathbf{x},\mathbf{y}) = \frac{1}{4\pi|\mathbf{r}|^3}\left[\hat{\mathbf{n}} - \frac{3(\hat{\mathbf{n}}\cdot\mathbf{r})\mathbf{r}}{|\mathbf{r}|^2}\right] \tag{43}$$

$$\mathbf{r} = \mathbf{y} - \mathbf{x}$$

The potential gradient distribution of the above-described problem is shown in figs. (15(a)), (15(b)) and (15(c)).

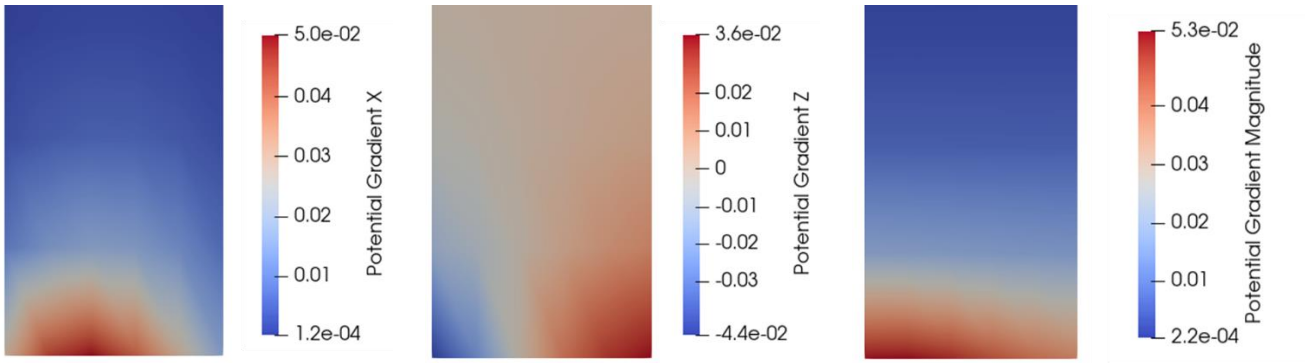

(a) (b) (c)

Figure 15*. a) Potential gradient distribution a) in x direction, b) in z direction, c) magnitude.*

From figs. 15 one can observe that the potential gradient is constant away from the metallic surfaces and varies close to the metallic surfaces. Thus, the integral equation of eq. (40) according to LD-BEM becomes:

$$c(\mathbf{x})c_1(\mathbf{x}) + \int_\Gamma P(\mathbf{x},\mathbf{y})c_1(\mathbf{y})d\Gamma = \int_\Gamma \Phi(\mathbf{x},\mathbf{y})\mathbf{n}\cdot\nabla c_1(\mathbf{y})d\Gamma - \frac{1}{D_1}\int_\Omega \Phi(\mathbf{x},\mathbf{y})\Delta\mathbf{v}_t\cdot\nabla c_1(\mathbf{y})d\Omega - \frac{1}{D_1}\int_\Omega \Phi(\mathbf{x},\mathbf{y})\dot{c}(\mathbf{y},t)d\Omega \tag{44}$$

with

$$
\begin{aligned}
&\Phi(\mathbf{x},\mathbf{y}) = G(\mathbf{x},\mathbf{y}) e^{-\frac{\bar{\mathbf{v}}_t\cdot(\mathbf{y}-\mathbf{x})}{2D_1}} = \frac{1}{2\pi}\mathrm{K}_0(sr) e^{-\frac{\bar{\mathbf{v}}_t\cdot\mathbf{r}}{2D_1}} \\
&P(\mathbf{x},\mathbf{y}) = \frac{\partial G(\mathbf{x},\mathbf{y})}{\partial \mathbf{n}_\mathbf{y}} e^{-\frac{\bar{\mathbf{v}}_t\cdot(\mathbf{y}-\mathbf{x})}{2D_1}} = -\frac{s}{2\pi}\mathrm{K}_1(sr)\left(\hat{\mathbf{r}}\cdot\mathbf{n}_\mathbf{y}\right) e^{-\frac{\bar{\mathbf{v}}_t\cdot\mathbf{r}}{2D_1}} \\
&s = \sqrt{\frac{k}{D_1} + \frac{\left(v_{t_x}\right)^2 + \left(v_{t_y}\right)^2}{4D_1^2}} \\
&\mathbf{v}_t = \bar{\mathbf{v}}_t + \Delta\mathbf{v}_t \\
&\mathbf{r} = \mathbf{y} - \mathbf{x}
\end{aligned}
\tag{45}
$$

where K_1 and K_0 are the modified Bessel functions of the second kind of first and zero order respectively.

The derivation of LD-BEM formulations for eq. (44), focusing on the numerical computation of the first volume integral of the right-hand side of the equation is currently one of the research interests of the author of the present work.

6. Conclusions

Dental implants corrode due their contact with saliva that disrupts the passive film, creating galvanic cells**.** The pairing of dissimilar materials for the dental implant body and suprastucture results in galvanic couples. Galvanic corrosion has adverse biological effects, including amongst others, bone destruction caused by the current flow that results from galvanic coupling, and allergic reactions or hypersensitivity reaction due the products of the alloy components dissolution, which can be distributed throughout the entire body. The boundary element method is ideal for solving galvanic corrosion problems due to the advantages of dimensionality reduction of the problem by one, and the high accuracy of the solution of the electric potential and concentration gradients. To solve efficiently, galvanic corrosion problems, the factors that influence the corrosion rate should be incorporated in the robin boundary conditions, since they are the most important parameter of the problem.

References

Al-Mayouf, A. M., Al-Swayih, A. A., Al-Mobarak, N. A., & Al-Jabab, A. S. (2004). Corrosion behavior of a new titanium alloy for dental implant applications in fluoride media. Materials Chemistry and Physics, 86(2), 320–329. https://doi.org/https://doi.org/10.1016/j.matchemphys.2004.03.019

Aoki, S., & Kishimoto, K. (1990). Application of BEM to Galvanic Corrosion and Cathodic Protection. In C. A. Brebbia (Ed.), Electrical Engineering Applications (pp. 65–86). Springer Berlin Heidelberg. https://doi.org/10.1007/978-3-642-48837-5_4

Balkin BE. Implant dentistry: historical overview with current perspective. Int J Oral Implantol. 1988;5(1):27-8. PMID: 3078244.

Böckris, J., Reddy, A., & Gamboa-Aldeco, M. (2000). Modern Electrochemistry, 2A: Fundamentals of Electrodics. second ed. Springer New York, NY, https://doi.org/10.1007/b113922

Brånemark, P.-I., Breine, U., Adell, R., Hansson, B. O., Lindström, J., & Ohlsson, Å. (1969). Intra-Osseous Anchorage of Dental Prostheses: I. Experimental Studies. Scandinavian Journal of Plastic and Reconstructive Surgery, 3(2), 81–100. https://doi.org/10.3109/02844316909036699

Danson, D.J., and Warne, M.A.: Current density/voltage calculations using boundary element techniques, Proc. Corrosion/83, Paper No. 211, 1983

Deconinck, J., Maggetto, G., & Vereecken, J. (1985). Calculation of Current Distribution and Electrode Shape Change by the Boundary Element Method. Journal of The Electrochemical Society, 132(12), 2960–2965. https://doi.org/10.1149/1.2113701

Flitt, H.J., Schweinsberg, D.P., 2005. A guide to polarisation curve interpretation: deconstruction of experimental curves typical of the Fe/H2O/H+/O2 corrosion system, Cor. Sci. 47(9), 2125-2156, https://doi.org/10.1016/j.corsci.2004.10.002.
Franck, U. F., Z. Naturforschung, 4A , 378 (1949).

Geis-Gerstorfer, J., Weber, H., & Sauer, K.H. (1989). In vitro substance loss due to galvanic corrosion in Ti implant/Ni-Cr supraconstruction systems. The International journal of oral & maxillofacial implants, 4 2, 119-23 .

Gortsas, T.V., Tsinopoulos, S.V., Polyzos., 2021. An accelerated boundary element method via cross approximation of integral kernels for large-scale cathodic protection problems. ComputAided Civ Inf. 1-16. https://doi.org/10.1111/mice.12687.

Gortsas, T. v, & Tsinopoulos, S. V. (2022). A local domain BEM for solving transient convection-diffusion-reaction problems. International Journal of Heat and Mass Transfer, 194, 123029. https://doi.org/https://doi.org/10.1016/j.ijheatmasstransfer.2022.123029

Gortsas, T. V, Tsinopoulos, S. V, & Polyzos, D. (2022). A local domain boundary element method for solving the nonlinear fisher KPP diffusion-reaction equation. Engineering Analysis with Boundary Elements, 138, 177–188. https://doi.org/https://doi.org/10.1016/j.enganabound.2022.02.008

Guglielmotti, M.B.; & Cabrini, R.L. (1997). Evaluación biológica de implantes dentales fracasados. Rev. Asoc. Odontol. Argent, 85, 313–317.

Gulikers, J., & Raupach, M. (2006). Numerical models for the propagation period of reinforcement corrosion - Comparison of a case study calculated by different researchers. Materials and Corrosion, 57(8), 618–627. https://doi.org/https://doi.org/10.1002/maco.200603993

Hines, J. G., 1983. Analysis of Complex Polarisation Curves, British Corrosion Journal, 18:1, 10-14, http://dx.doi.org/10.1179/000705983798274001.

Kalovelonis, D. T., Gortsas, T. V., Tsinopoulos, S. V., & Polyzos, D. (2022). Optimal Design of a Sacrificial Anode Cathodic Protection System for an Offshore Wind Turbine Jacket Foundation via Accelerated BEM, No 44, 13th congress of Hellenic Society of Theoretical and applied mechanics, Stavroulakis, G.E., Polyzos, D., & Hatzigeorgiou, G.D. (ed.), Patras, Greece. ISSN / E-ISSN: / 2944-9359, ISBN/ 978-960-530-181-1

Kalovelonis, D. T., Gortsas, T. v., Tsinopoulos, S. v., & Polyzos, D. (2022). Accelerated boundary element method for direct current interference of cathodic protections systems. Ocean Engineering, 258, 111705. https://doi.org/10.1016/j.oceaneng.2022.111705

Kalovelonis, D.T., Rodopoulos, D.C., Gortsas, T.V., Tsinopoulos, S.V., Polyzos, D., 2020. Cathodic protection of a container ship using a detailed BEM model. J. Mar. Sci. Eng. 8, 359-373 https://doi.org/10.3390/jmse8050359.

Kalovelonis, D. T., Gortsas, T. V., Tsinopoulos, S. V. (2023). Modelling of 3D periodic cathodic protection problems in reinforced concrete structures with accelerated Boundary Element Method. Under revision at Construction and Building Materials, Elsevier.

Kandavalli, S. R., Wang, Q., Ebrahimi, M., Gode, C., Djavanroodi, F., Attarilar, S., & Liu, S. (2021). A Brief Review on the Evolution of Metallic Dental Implants: History, Design, and Application. Frontiers in Materials, 8. https://www.frontiersin.org/articles/10.3389/fmats.2021.646383

Keddie, A.J., Pocock, M.D., DeGiorgi, V.G., 2007. Fast solution techniques for corrosion and signatures modelling, in: Brebbia, C. A. (Ed.), WIT Transactions on Engineering Sciences vol 54, WIT Press, Southampton, pp. 225-234. https://doi.org/10.2495/ECOR070221.

King, P.,Uhlig, H. , J. Phys. Chem, 63 , 2026 (1959)

Kubie, L.S., & Shults, G.M. (1925). STUDIES ON THE RELATIONSHIP OF THE CHEMICAL CONSTITUENTS OF BLOOD AND CEREBROSPINAL FLUID. The Journal of Experimental Medicine, 42, 565 - 591.

Liu, Y.J., 2009. Fast Multipole Boundary Element Method: Theory and Applications in Engineering, Cambridge University Press.

Lucas, L. C., & Lemons, J. E. (1992). Biodegradation of Restorative Metallic Systems. Advances in Dental Research, 6(1), 32–37. https://doi.org/10.1177/08959374920060011301

Macdonald, D.D., Qiu, J., Zhu, Y., Yang, J., Engelhardt, G.R., Sagüés, A., 2020. Corrosion of rebar in concrete. Part I: Calculation of the corrosion potential in the passive state, Cor.Sci. 177, 109018. https://doi.org/10.1016/j.corsci.2020.109018

Macdonald, D.D., Zhu, Y., Yang, J., Qiu, J., Engelhardt, G.R., Sagüés, A., Sun, L., Xiong, Z., 2021. Corrosion of rebar in concrete. Part IV. On the theoretical basis of the chloride threshold, Cor. Sci. 185, 109460. https://doi.org/10.1016/j.corsci.2021.109460.

Manivasagam, G., Dhinasekaran, D., & Rajamanickam, A. (2010). Biomedical Implants: Corrosion and its Prevention - A Review. Recent Patents on Corrosion Science, 2(1), 40–54. https://doi.org/10.2174/1877610801002010040

Mellado-Valero, A., Muñoz, A., Pina, V., & Sola-Ruiz, M. (2018). Electrochemical Behaviour and Galvanic Effects of Titanium Implants Coupled to Metallic Suprastructures in Artificial Saliva. Materials, 11(1), 171. https://doi.org/10.3390/ma11010171

Nagay, B. E., Cordeiro, J. M., & Barao, V. A. R. (2022). Insight Into Corrosion of Dental Implants: From Biochemical Mechanisms to Designing Corrosion-Resistant Materials. Current Oral Health Reports, 9(2), 7–21. https://doi.org/10.1007/s40496-022-00306-z

Nakayama, A., Sano, Y., Bai, X., & Tado, K. (2017). A boundary layer analysis for determination of the limiting current density in an electrodialysis desalination. Desalination, 404, 41–49. https://doi.org/https://doi.org/10.1016/j.desal.2016.10.013

Newman, J., Thomas-Alyea, K.E., 2004. Electrochemical Systems. third ed. John Wiley & Sons, New Jersey.

Olmedo, D., Fernández, M. M., Guglielmotti, M. B., & Cabrini, R. L. (2003). Macrophages Related to Dental Implant Failure. Implant Dentistry, 12(1), 75–80. https://doi.org/10.1097/01.ID.0000041425.36813.A9

Peers, A. M., General Discussion, Discuss. Faraday Soc. 21 (1956) 124.

D. Polyzos, S.V. Tsinopoulos, D.E Beskos, 1998. Static and dynamic boundary element analysis in incompressible linear elasticity, Eur J Mech A Solids, 17 (3), 515-536.

Popov, B.N., 2015. Corrosion Engineering Principles and Solved Problems. Elsevier, Amsterdam

Pourbaix, M., Atlas of Electrochemical Equilibria in Aqueous Solutions, 2nd Ed., NACE, Houston, TX, 1974

Revie, R.W., Uhlig, H.H., 2008. Corrosion and corrosion: control an introduction to corrosion science and engineering. John Wiley & Sons

Rocha, H., & Lennartz, G., Arch. Eisenhüttenw . 26 , 117 (1955).

Rodopoulos, D.C., Gortsas T.V., Tsinopoulos, S. V., Polyzos, D., 2019. ACA/BEM for solving large-scale cathodic protection problems. Eng. Anal. Bound. Elem. 106, 139-148. https://doi.org/10.1016/j.enganabound.2019.05.011.

Scales, J. T., Winter, G. D., & Shirley, H. T. (1959). Corrosion of orthopaedic implants: screws, plates and femoral nail-plates. The Journal of Bone and Joint Surgery. British volume, 41(4), 810-820.

Telles, J.C.F., W.J. Mansur, and L.C. Wrobel, 1984. On boundary elements for external potential problems. Mechanics Research Communications 11(6), 373-377. https://doi.org/10.1016/0093-6413(84)90044-2

Venugopalan, R., & Lucas, L. C. (1998). Evaluation of restorative and implant alloys galvanically coupled to titanium. Dental Materials, 14(3), 165–172. https://doi.org/https://doi.org/10.1016/S0109-5641(98)00024-4

Williams, D. F. (1987). Tissue-biomaterial interactions. Journal of Materials Science, 22(10), 3421–3445. https://doi.org/10.1007/BF01161439

Warkus, J., & Raupach, M. (2006). Modelling of reinforcement corrosion – Corrosion with extensive cathodes. Materials and Corrosion, 57(12), 920–925. https://doi.org/https://doi.org/10.1002/maco.200604032

Warkus, J., & Raupach, M. (2010). Modelling of reinforcement corrosion – geometrical effects on macrocell corrosion. Materials and Corrosion, 61(6), 494–504. https://doi.org/https://doi.org/10.1002/maco.200905437

Wrobel, L.C.,2002, The Boundary Element Method, Volume 1: Application in Thermo-Fluids and Acoustics, Wiley, UK.